applied optics

High-contrast pattern reconstructions using a phase-seeded point CGH method

Richard McWilliam,[1,*] Gavin L. Williams,[2] Joshua J. Cowling,[3] Nicholas L. Seed,[2] and Alan Purvis[1]

[1]School of Engineering and Computing Sciences, Durham University, Science Laboratories, South Road, Durham, DH1 3LE, UK
[2]Electronic and Electrical Engineering Department, University of Sheffield, Sheffield, S1 3JD, UK
[3]Ibex Innovations, Discovery 2, NETPark, Sedgefield, Durham, TS21 3FH, UK
*Corresponding author: r.p.mcwilliam@durham.ac.uk

Received 1 September 2015; revised 17 January 2016; accepted 19 January 2016; posted 19 January 2016 (Doc. ID 248764); published 26 February 2016

A major challenge encountered in digital holography applications is the need to synthesize computer-generated holograms (CGHs) that are realizable as phase-only elements while also delivering high quality reconstruction. This trade-off is particularly acute in high-precision applications such as photolithography where contrast typically must exceed 0.6. A seeded-phase point method is proposed to address this challenge, whereby patterns composed of fine lines that intersect and form closed shapes are reconstructed with high contrast while maintaining a phase-only CGH. The method achieves superior contrast to that obtained by uniform or random seeded-phase methods while maintaining computational efficiency for large area exposures. It is also shown that binary phase modulation achieves similar contrast performance with benefits for the fabrication of simpler diffractive optical elements.

OCIS codes: (090.1995) Digital holography; (110.5220) Photolithography; (230.6120) Spatial light modulators.
http://dx.doi.org/10.1364/AO.55.001701

1. INTRODUCTION

Computer-generated holograms (CGHs) are finding use in many applications where conventional imaging systems are not able to provide the required performance. Examples include optical data storage, beam shaping of high power laser beams, three-dimensional optical tweezers for microscopy, displays, and photolithography. Each of these exploits one or more capabilities offered by CGH imaging. The ability to modulate the phase of incident illumination enables efficient reconstruction of both planar and nonplanar features.

A major challenge in the deployment of digital holography is the need to quantize the CGH distribution into a discrete set of amplitude and/or phase values, driven by the fact that complex modulation is not practical using currently available photomasks and spatial light modulator (SLM) devices. This modification introduces noise into the reconstructed image and hence results in poor image contrast.

For some applications the error incurred is tolerable and thus further refinement of the CGH is unnecessary. An example is the case of displays, where characteristics of the human visual system may be exploited in order to reduce error requirements and hence increase computational efficiency [1]. However, precision imaging applications such as photolithography demand that refinements be made. An example of this is the introduction of time averaging of multiple exposures using an SLM device in order to reduce noise in the reconstruction [2]. Other methods based on the Fresnel cylindrical lens (FCL) or Fresnel zone plate (FZP) achieve good performance under certain conditions.

Iterative solutions have been used in instances where the CGH must be restricted to a phase-only distribution. This is often implemented as the Gerchberg–Saxton algorithm [3], involving successive reduction of errors appearing within the reconstruction when imposing the phase-only restriction in the CGH. There are examples of high-quality reconstructions being achieved by error reduction methods based on iterative Fourier transform methods (IFTMs) [4] including generation of nonplanar patterns [5]. While many refinement methods exist [6], limitations remain concerning the handling of "Manhattan" geometry patterns composed of lines that intersect and abut one another. With "thin" features comparable to the full width at half-maximum (FWHM) of the point-spread function of the optical system, a special case exists where iterative algorithms can, when properly seeded and accurately sampled, begin to normalize out features such as the severe spikes found at line terminations and intersections [7]. These features are normally present in analytical approximations to thin patterns and can be devastating where consistent high-contrast patterns are required, such as in the application of photolithography, resulting in complex mask requirements to minimize such variations.

In this paper, a point method is proposed wherein the CGH is composed of multiple superimposed FZP diffraction patterns without iterative refinement. Instead, the CGH is calculated in a single step and is immediately reduced to a phase-only format. A novel phase-seeded method is defined with the aim of rendering the CGH more amenable to the phase restriction step. The approach also seeks to address the problem of reproducing patterns composed of intersecting and multisegment lines, which are commonly encountered in microlithography. This is achieved by preseeding the phase of each point source within the object according to a distribution function, followed by direct generation of the CGH.

To devise a point-oriented method suitable for the purpose of photolithography, two modifications are applied. First, a predetermined phase function is applied to the point-oriented object (without further refinement) in order to improve contrast. Second, continuity of line patterns is secured by ensuring that the point-oriented object is sampled at an interpoint spacing below that of the FWHM of the PSF of the CGH. By reducing the side effects incurred by discarding amplitude information, the resulting CGH reconstruction is shown to display significant improvements in image contrast. It is also proposed that the same analytical phase modification may be applied to a variety of pattern geometries, therefore creating an efficient CGH generation algorithm without the need for calculating multiple seed-phase functions.

The structure of the remainder of the paper is as follows. Section 2 considers existing methods and identifies their limitations. Section 3 develops the point CGH and seeded-phase methods. Section 4 goes on to develop a method for analyzing the seeded-phase method according to a contrast metric, then presents example results generated by the method including a comparison with IFTM-generated reconstructions. Section 5 presents experimental confirmation of the approach. Finally, conclusions are drawn in Section 6.

2. EXISTING METHODS

FCL methods have been used to reconstruct lines with high positional accuracy for visual display [8] and high-contrast photolithography [9]. A parameterized approach is taken whereby each line segment is assigned a CGH derived from the FCL function:

$$H(u,v) = \exp\left(\frac{jkv^2}{2z}\right)\mathrm{rect}(L_u, L_v), \tag{1}$$

where z is the reconstruction distance and k is the wave number. Each CGH is further truncated to a rectangle of dimensions L_u, L_v by the rect function. Figure 1 illustrates an example of the typical line pattern reconstructed by the FCL method. Although singular line patterns can be successfully reconstructed, intersecting and abutted features, such as those illustrated in Fig. 2, are severely degraded even when the full complex CGH is retained. An example of this is illustrated in Fig. 3, where the complex CGH reproduces poor line quality. Further degradation occurs if the CGH amplitude is also discarded.

Modifications have been proposed to improve line quality by including Fresnel diffraction function (FDF) terms into the parameterized line FCL equation [10]:

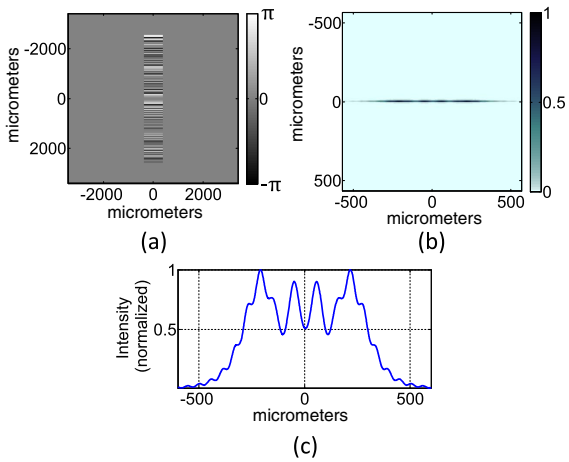

Fig. 1. Geometry of line and example reconstruction by FCL for a target line length of 760 μm. (a) CGH phase. (b) Intensity of reconstructed pattern. (c) Horizontal intensity profile.

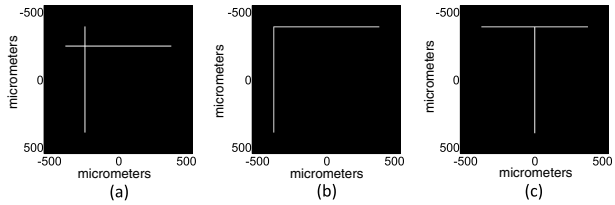

Fig. 2. Examples of troublesome pattern geometries.

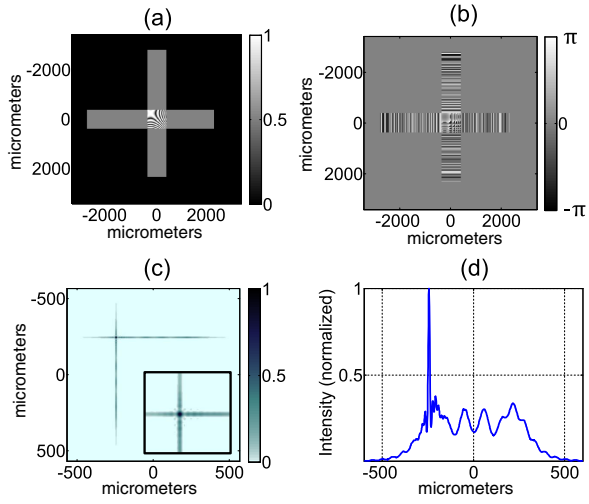

Fig. 3. Illustrative example of pattern degradation for intersecting line pattern when using the FCL method. (a) CGH amplitude. (b) CGH phase. (c) Intensity of reconstructed pattern (inset showing magnified image of intersection region). (d) Profile of horizontal line intensity.

$$H(u,v) = \exp\left(\frac{jkv^2}{2z}\right)F(u)\mathrm{rect}(L_u, L_v), \tag{2}$$

where $F(u)$ is the FDF:

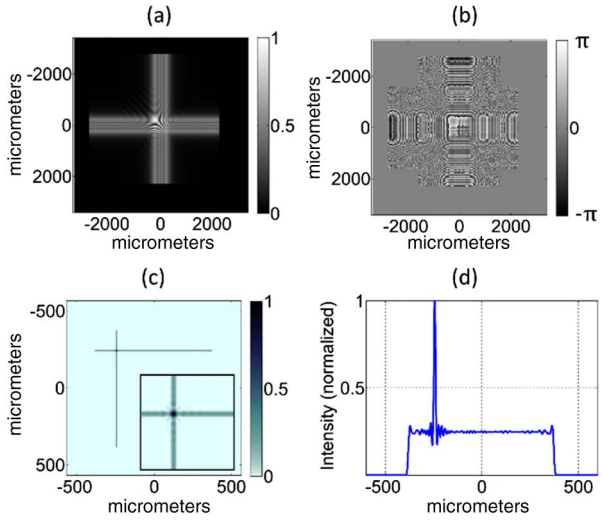

Fig. 4. Pattern degradation when using the FCL–FDF method. (a) CGH amplitude. (b) CGH phase. (c) Intensity of reconstructed pattern (inset showing magnified image of intersection region). (d) Profile of horizontal line intensity.

$$F(u) = \frac{1}{\sqrt{2}} \int_{a2}^{a1} \exp\left(j\frac{\pi}{2}a^2\right) \mathrm{d}a, \tag{3}$$

with the limits of integration given by

$$a1 = -\sqrt{\frac{2}{\lambda Z}}\left(\frac{L}{2} + u\right), \qquad a2 = \sqrt{\frac{2}{\lambda Z}}\left(\frac{L}{2} - u\right). \tag{4}$$

The FCL–FDF method brings significant improvements in line quality, but requires complex modulation for both single and multiple line patterns. Furthermore, intersections are still problematic in that strong peaks are present at the point of intersection, as illustrated in Fig. 4. This is undesirable in photolithography because significant energy is contained within the peak, reducing the intensity in other regions of the line. Contrast is therefore reduced, with the result that exposure conditions become difficult to control. As with the FCP method, further degradation occurs when discarding the CGH amplitude. The parameterized FCL–FDF approach is therefore of limited scope when phase-only CGHs are sought.

3. SEEDED-PHASE METHOD

Our approach is based on a modified point CGH method incorporating a preseeded object phase [11]. The point method has previously been demonstrated to generate patterns in two- and three-dimensional space [12].

A. Point Model

The basic point model adopted assumes that the object is composed of a distribution of point sources, each accounted for in the CGH by their respective offset FZP diffraction pattern:

$$\mathrm{FZP}(u, v{:}x_n, y_m) = \exp\left\{\frac{jk}{2z}[(u - x_n)^2 + (v - y_m)^2]\right\} \mathrm{circ}(x_n, y_m, r), \tag{5}$$

where x_n, y_m are the offset locations of each point in the object plane, typically stored in vector form as a collection of discrete values. The circ function limits the extent of each FZP contribution to a circle of radius r according to

$$\mathrm{circ}(x_n, y_m, r) = \begin{cases} 1 & \sqrt{(u - x_n)^2 + (v - y_m)^2} \le r \\ 0 & \sqrt{(u - x_n)^2 + (v - y_m)^2} > r \end{cases}. \tag{6}$$

The complete CGH results from the summation of all individual FZP contributions:

$$H(u, v) = \sum_{n,m} \mathrm{FZP}(u, v{:}x_n, y_m). \tag{7}$$

For sparse line patterns spanning large exposure areas, this approach can become extremely efficient in comparison to Fourier methods since n, m relate to the number of object points rather than the field extent. Thus the computational burden of FZP methods is dictated by the degree of sparsity in the point representation of the object. Point methods also allow direct modification of the relative phase of each point source, a technique referred to here as phase seeding.

Referring to Fig. 5, the specified input pattern is described as some real-valued function $O(x, y)$ contained within the reconstruction plane and in which lines are restricted to a single point width. From this, a discrete collection of point locations is generated and stored in matrix T:

$$T_{n,m} = \sum_{n=1}^{N} \sum_{m=1}^{M} O(x, y)\delta(x - n\Delta x, y - m\Delta y). \tag{8}$$

Parameters n, m are the array indices of t, δ is the two-dimensional Dirac function, N and M are the number of samples in the horizontal and vertical directions, respectively, and $\Delta x, \Delta y$ are the horizontal and vertical object point spacing, respectively. Alternatively, $T_{n,m}$ may be specified directly from an existing discrete point distribution. A complex object point representation $Q_{n,m}$ is then generated by assigning phase values stored in matrix $\psi_{n,m}$:

$$Q_{n,m} = T_{n,m} \exp(j\psi_{n,m}). \tag{9}$$

The complete CGH is finally built up from the summation of all point contributions:

$$H(u, v) = \left(\frac{1}{A}\right) \sum_{n,m} [Q_{n,m} \mathrm{FZP}(u, v{:}x_n, y_m)] \mathrm{rect}\left(\frac{u}{L_u}, \frac{v}{L_v}\right), \tag{10}$$

where A is a normalization factor given by $A = \Sigma_{n=1}^{N} \Sigma_{m=1}^{M} |T_{n,m}|$, and the CGH is once more limited in extent by a rect function. Note that the FZP function is typically

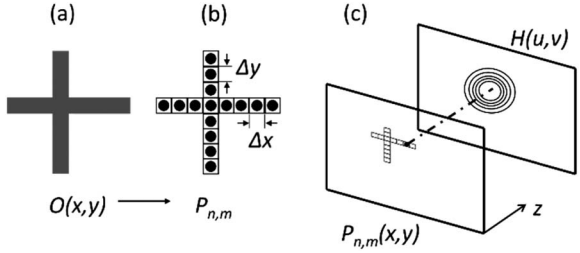

Fig. 5. Geometry used for point method. (a) Idealized line pattern shape. (b) Point-oriented representation of pattern. (c) Coordinate planes for the CGH and object.

discretized according to the required sampling conditions in the CGH, in which case Eq. (10) yields the discrete CGH.

B. Seeded-Phase Function

Direct manipulation of the quantized CGH (and therefore its phase-quantized performance) is possible by careful assignment of the object phase distribution $\psi_{n,m}$. One strategy is to randomize the object phase distribution in order to average the strongest interference peaks and troughs. However, this approach still does not yield adequate imaging quality for the purposes of precision applications such as photolithography. Observations made in [13] showed that, under different conditions, a class of analytical object phase functions could be used to reduce noise present in the optical reconstruction. More recently, strategies have included the use of interpolated pseudo-random phase distributions [14] and CGH composed of multiple offset point-oriented patterns [15]. Self-transforming functions, i.e., those functions whose Fourier transform takes a similar form, were observed to alleviate interference effects produced by quantized Fourier holograms [13]. An alternative function is chosen here that takes the form of a scaled FZP:

$$\varphi(x,y) = \frac{\pi\alpha}{\lambda z}(x^2 + y^2), \tag{11}$$

where the constant α modifies the radial positions of the associated phase fringes. The equivalent sampled phase distribution $\psi_{n,m}$ is generated by sampling in the same manner as is done for Eq. (8). Examples of the effect of choosing different α are illustrated in Fig. 6, where a smoothing of the CGH amplitude is observed for the object illustrated in Fig. 2(a).

In summary, the following seed-phase methods are compared:

(1) when $\psi_{n,m}$ is assigned the distribution of Eq. (11), varying α between the integer range 1…7;
(2) when $\psi_{n,m}$ is assigned the uniform value of zero;
(3) when $\psi_{n,m}$ is assigned a random phase distribution $\varphi(x,y) = \text{rand}\{0,1\} \cdot 2\pi$, where rand{0, 1} generates uniform random numbers over the interval 0…1; and

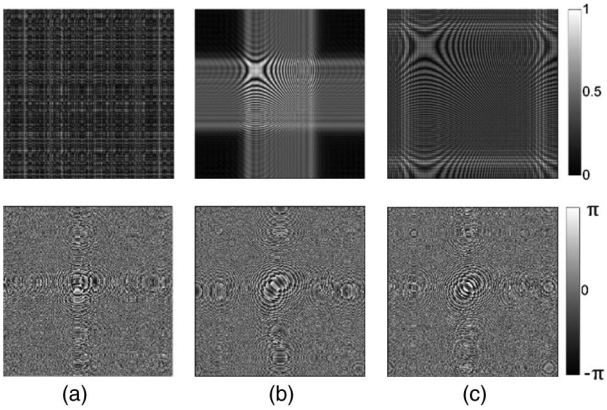

Fig. 6. Examples of CGHs produced by the seeded-phase method. The top row shows normalized CGH amplitude. The bottom row shows CGH phase. Methods shown are: (a) uniform random phase, (b) analytical phase with $\alpha = 3$, and (c) analytical phase with $\alpha = 7$.

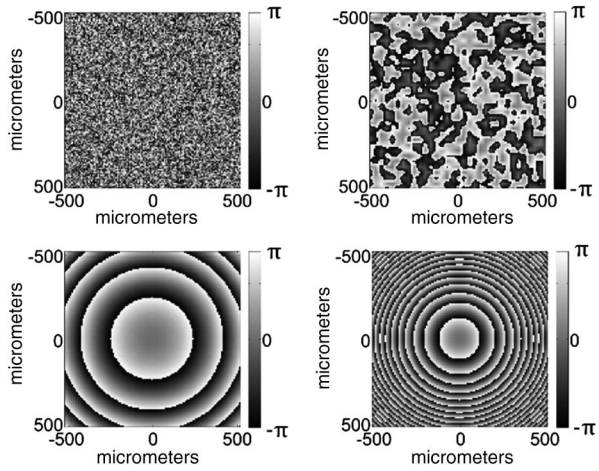

Fig. 7. Illustration of seeded-phase distributions applied to point object pattern. Clockwise from top left: uniform random, pseudo-random ($p = 4$), analytical ($\alpha = 4$), and analytical ($\alpha = 1$).

(4) when $\psi_{n,m}$ is assigned an interpolated random phase distribution created by inserting p interpolated values between an initial random sequence. The initial random sequence should be p times smaller than the final pseudo-random sequence. For $p = 1$ the original pseudo random sequence remains and for $p > 1$ a progressively smoother phase distribution is generated.

Examples of each seeded-phase method are illustrated in Fig. 7.

4. COMPARATIVE ANALYSIS

Since patterns composed of single isolated lines may be dealt with by the FCL method, we concentrate here on patterns composed of intersecting and abutted features of the types illustrated in Fig. 2. For the pattern shown in Fig. 2(a), reconstructed patterns are calculated by simulation for each seeded-phase method. Key parameters used in simulations are summarized in Table 1. For each point method, the CGH was calculated using Eq. (10) evaluated over a grid of 850 × 850 pixels and the subsequent reconstructed intensity field by a fast Fourier transform (FFT)-based Rayleigh–Sommerfeld propagation [16] sampled at 1 μm to ensure high accuracy. Each complete line pattern is composed of 255 discrete points and, in order to generate smooth reconstructed features, the object point spacing is set to be less than the CGH sample spacing.

The influence of different seeded-phase methods is illustrated in Fig. 8, where various reconstructions are compared for the same input pattern. The simulation results for each

Table 1. Summary of Design Parameters Used for Evaluation

Parameter	Value
Wavelength, λ	405 nm
CGH sampling	8 μm
Propagation sampling	1 μm
Object sampling, $\Delta x, \Delta y$	6 μm
Reconstruction distance, z	8 cm

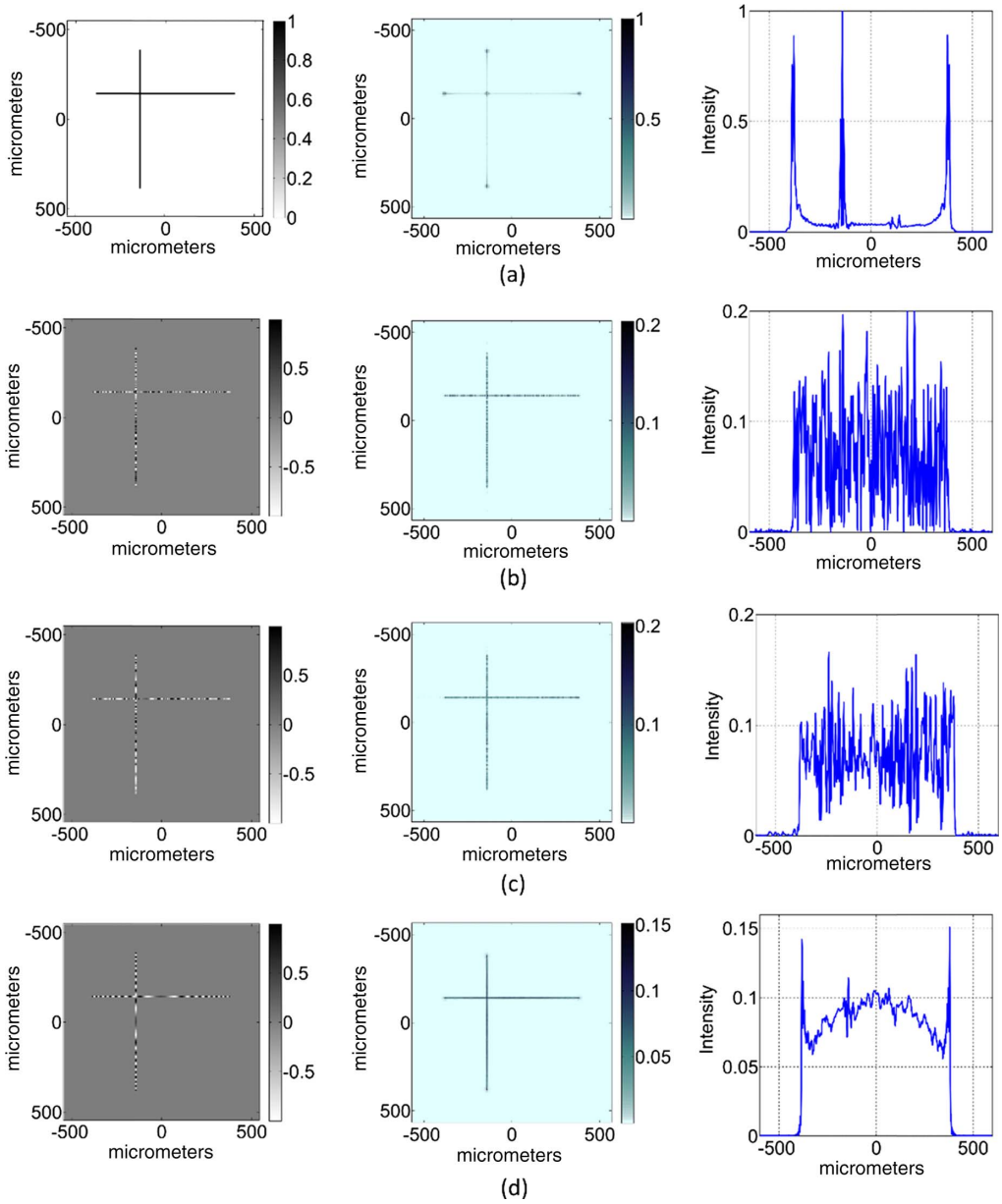

Fig. 8. Simulated pattern reconstructions for different object seeded-phase methods. The left column shows the real part of point object distribution after addition of seeded phase; the middle column shows a 2D image of the reconstructed pattern intensity; the right column shows a cross-sectional plot of the reconstructed intensity taken along a horizontal line. (a) Uniform phase. (b) Uniform random phase. (c) Pseudo-random phase method ($p = 2$). (d) Analytical method ($\alpha = 4$). All intensity graphs are normalized relative to a uniform phase result.

method are summarized in the form of 2D intensity patterns and cross-sectional intensity plots. The uniform phase method displays severe degradation similar to the FCL–FDF method in that significant peaks exist within the line profile. The uniform random phase result exhibits clearly defined boundaries demarcating the line pattern, but substantial noise remains within the line profile. For the pseudo-random phase method various values for p were evaluated, and the best result was obtained for $p = 2$. A small improvement in noise floor is seen; however, the latitude for exposure adjustment is extremely narrow. For the analytical case ($\alpha = 4$), a smoothing of the CGH amplitude occurs and hence the CGH yields to phase-only conversion.

The analytical approach was explored further by re-evaluating the procedure for various α. The results are displayed in Fig. 9, where, for variety, a different pattern has been defined. It is seen that performance degrades for $\alpha < 4$, and, hence, an optimal value appears to exist for the optical parameters used.

The method is not restricted to single intersections; an example of a square outline geometry is illustrated in Fig. 10, where significant improvements are again brought by applying the seeded-phase method.

A. Contrast Analysis

To further assess the usefulness of the seeded-phase method, a contrast metric is proposed for strict evaluation [17]:

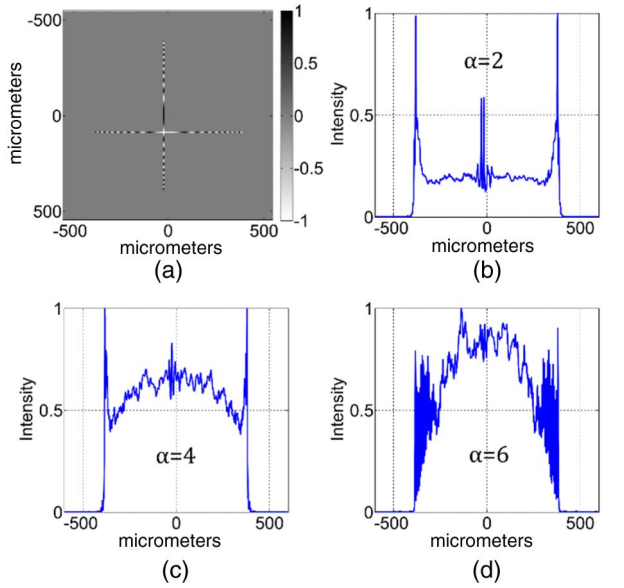

Fig. 9. Comparison of cross-sectional reconstructions using the analytical method. (a) Real part of the point object distribution (shown for $\alpha = 4$). (b)–(d) Cross-sectional plots of the reconstructed intensity for various α.

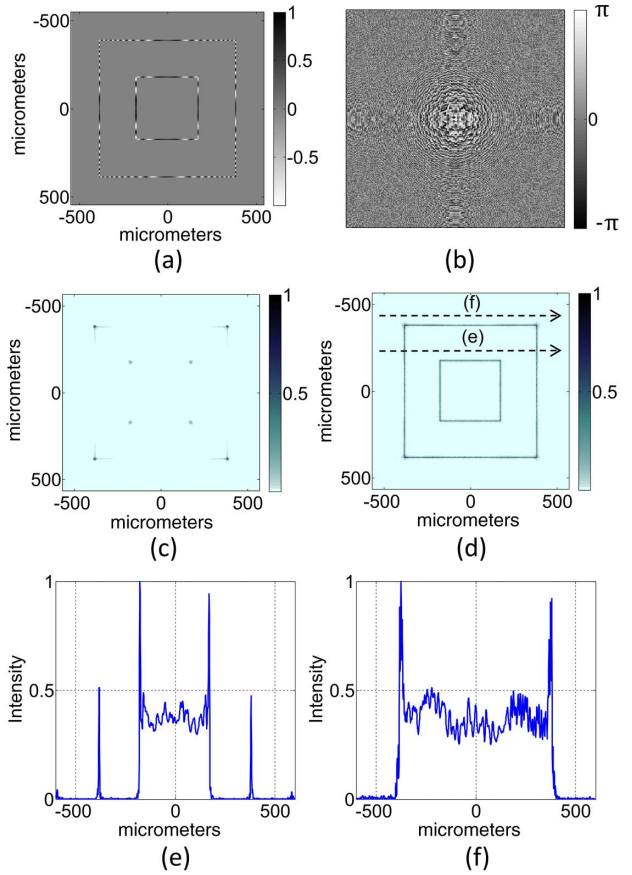

Fig. 10. Example of square pattern reconstruction. (a) Seeded-phase object (real part). (b) CGH. (c) Reconstruction resulting from the uniform phase method. (d) Reconstruction resulting from the analytical phase method ($\alpha = 4$). (e) Cross-sectional intensity profiles along the inner/outer squares.

$$C = \frac{I_{\min} - I_{\max}}{I_{\max} + I_{\min}}, \tag{12}$$

where $I_{\max}$ is the maximum intensity occurring with the background region (i.e., lying outside of the region of the pattern) and $I_{\min}$ is the minimum intensity occurring within the region of the pattern. With reference to Fig. 11, evaluation is further refined by dividing the cross-sectional intensity profile into three regions comprising background, transition, and midsection zones. Contrast is not evaluated within the transition zones since they contain the sharply rising sidewall peaks that demarcate the end points of each line—a feature that is considered desirable in photolithography. These typically reach a peak overshoot intensity greater than the midsection zone and hence could bias the contrast measurement.

To determine the design sensitivity of the seeded-phase parameters, contrast is evaluated for various patterns, each produced using various values of α. The results are summarized in Fig. 12, where sets of contrast results are displayed for each pattern. In all cases the excluded transition zones each comprise 5% of the total line profile, and, hence, $I_{\min}$ is evaluated over 90% of the complete line profile. It can be seen that, using the phase function of Eq. (11), the highest contrast figure is attained for $\alpha = 4$. For these cases contrast far exceeds the typical criteria of $C > 0.6$ for photolithography [17]. In general, useful contrast is seen for $2 \leq \alpha \leq 6$.

Comparative results were also evaluated for the case where the CGH is restricted to binary phase values and included in Fig. 12. A remarkably similar behavior is observed, most likely attributed to the use of patterns composed of thin lines. An additional comparison is made by including the pseudo-random phase method where p is varied between the same range as that for α. In this case, limited improvements are observed; however, contrast is in general below that required for photolithography purposes. The results suggest that binary phase CGHs compare favorably with their multiphase level counterparts, and that, although diffraction efficiency is reduced for binary phase modulation, the fabrication of CGH in the form of diffractive optical elements is simplified considerably.

B. Comparison with Iterative Method

Comparison IFTM results were generated by sampling each target pattern at 1 μm in order to produce the same reconstruction resolution as with the point method (see Table 1). An efficient angular spectrum (AS) propagation algorithm was used as

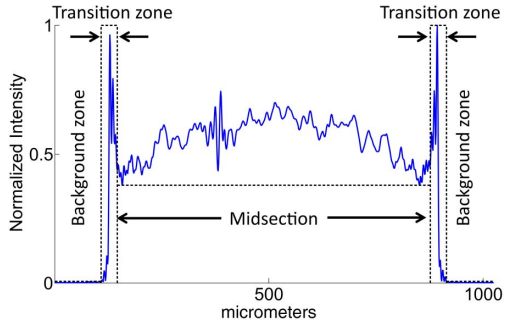

Fig. 11. Measurement zones for determining contrast of the line intensity profile.

described in [5] but applied here to the two-dimensional case under consideration. The use of FFTs requires that sampling of the CGH be equivalent to that of the object (i.e., 1 μm in this case) and additional paddingof the CGH in order to avoid aliasing of the transfer function. This represents a significant computational memory increase in comparison to the point method, which generates the CGH at sample pitch of 8 μm by direct evaluation of Eq. (10).

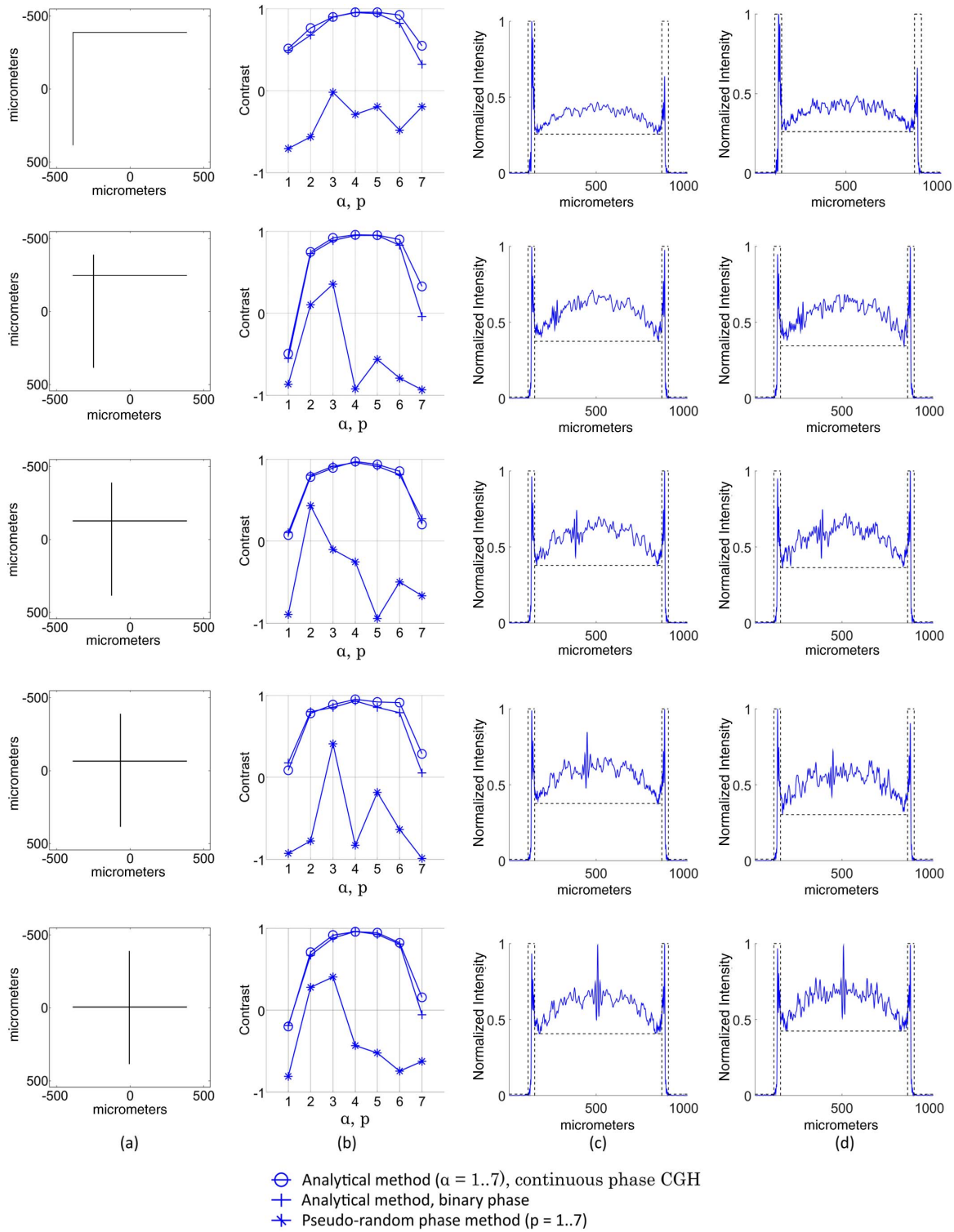

Fig. 12. Distribution of contrast for two lines intersecting at various locations. Column (a): object patterns. Column (b): contrast results for the analytical seeded-phase and pseudo-random phase methods. Column (c): cross-sectional plots of the reconstructed intensity profile for $\alpha = 4$ and continuous phase CGH. Column (d): cross-sectional plots of the reconstructed intensity profile for $\alpha = 4$ and binary phase CGH. All intensity results are individually normalized.

The resulting IFTM profiles and contrast results are presented in Fig. 13, for which contrast was evaluated on an identical basis as for the point method (Fig. 12). The IFTM was terminated after 10 iterations, beyond which any further increase of contrast was observed to be minimal. Due to the fine-pitch sampling of the target pattern, high contrast is observed for continuous phase CGHs, exceeding 0.94 in all cases. However, an appreciable reduction in contrast is seen when further restricting the CGH to binary phase form, and troublesome peaks manifest at the points of line intersection. Although further optimization of the IFTM may be possible, the point method is comparatively robust to binarization of CGH phase. Regarding practical computation considerations, three observations may be made: first, the point method operates on a sparse object pattern representation rather than a regularly sampled field. Second, the object and CGH field parameters (sample

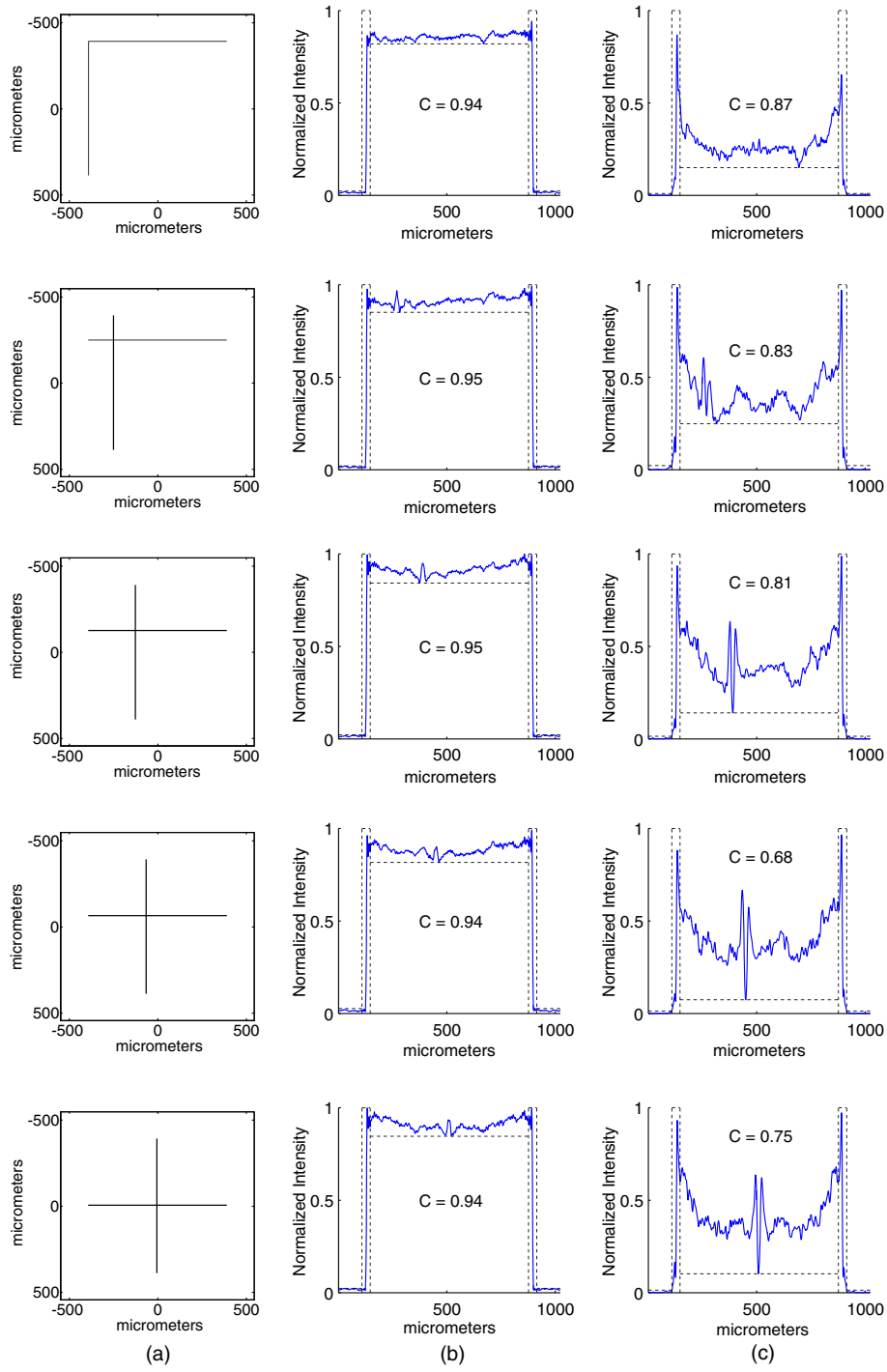

Fig. 13. Comparative results generated using the IFTM method, where contrast C for each case is indicated within the respective plot. Column (a): object patterns (as per Fig. 12). Column (b): cross-sectional plots of the reconstructed intensity profile using a continuous phase CGH. Column (c): cross-sectional plots of the reconstructed intensity profile using binary phase CGH. IFTM results were generated using 10 iterations.

Table 2. Contrast Analysis for Detailed Study

Contrast Metric	Value
Maximum	0.98
Minimum	0.84
Mean	0.95
Standard deviation	0.01

pitch and size) become decoupled. Finally, the CGH is generated directly, and no iteration is required.

C. Sensitivity Analysis

Returning to the point method, the results presented in Fig. 12 demonstrate that contrast remains well behaved for a range of pattern geometries. In particular, the optimal condition $\alpha = 4$ holds for generalized intersections involving two lines. To further determine the stability of this result, a detailed study of contrast versus pattern geometry was conducted. Referring to Fig. 14, a series pattern was generated, each composed of two orthogonal lines intersecting at all locations coinciding with a 128 × 128 grid. Setting $\alpha = 4$ in each case (other parameters set per Table 1), a high degree of uniformity is observed, as summarized in Table 2, with the condition $C > 0.6$ holding in all cases. The contrast values attained are also plotted in Fig. 14.

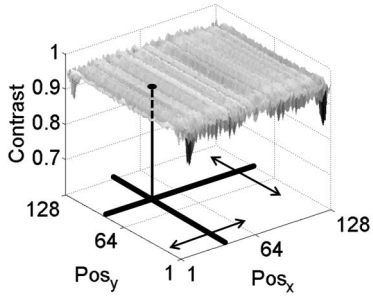

Fig. 14. Procedure for analysis of contrast performance for different line intersection locations and a continuous phase CGH calculated by the point method. For each result, the location of the line intersection is altered within a 128 × 128 grid spaced by 6 μm.

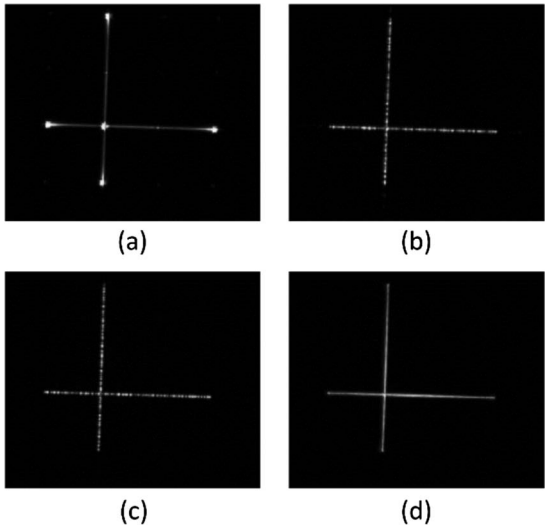

Fig. 15. Experimental LCOS reconstruction of patterns. (a) Uniform-phase method. (b) Uniform random phase method. (c) Pseudo-random phase method ($p = 3$). (d) Seeded-phase method ($\alpha = 4$).

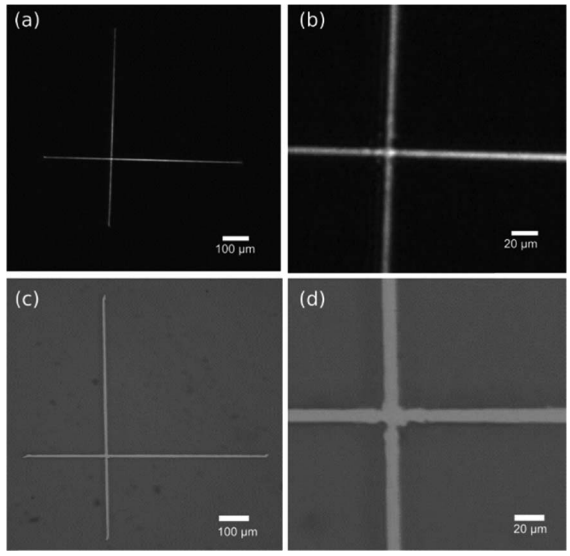

Fig. 16. Experimental results. (a) SLM reconstruction with (b) enlarged view. (c) Metal tracks generated following photoresist exposure and (d) close-up view of the track intersection.

5. EXPERIMENTAL RESULTS

We demonstrate the resulting image quality achieved by experimental photolithography exposure. Photolithography is extremely sensitive to pattern defects and demands high contrast. It is, therefore, a good means of evaluating the success of the method. Reconstructed patterns were generated using a reflective phase-only SLM (Holoeye Pluto, 850 × 850 active array of pitch 8 μm) and a diode laser operating at 405 nm. Further details of the holographic photolithography apparatus can be found in [18]. Figure 15 shows four examples of patterns generated using the various seeded-phase methods considered in Section 3 captured by digital camera sensor. Each example exhibits similar features, as previously observed in Fig. 8.

The seeded-phase method was then tested within an experimental holographic photolithography system. A phase CGH was again generated as a 256-level phase-only CGH seeded with an analytical phase function ($\alpha = 4$) and displayed via SLM. Figures 16(a) and 16(b) illustrate the intensity observed at the imaging plane. Positive-acting photoresist was then exposed and developed, followed by a metal lift-off process used to convert the resulting pattern into gold tracks, as shown in Figs. 16(c) and 16(d). Reduction in overall line width near the intersection point can be seen; however, the tracks are continuous and there are no spurious features, thus confirming the high-contrast reproduction.

6. CONCLUSIONS

The point-oriented approach offers the attractive proposition of realizing "Manhattan" line patterns with intersections over large-area substrates. The computational burden is primarily

dependent upon the pattern complexity rather than field size. However, the resulting CGH does not yield easily to continuous or binary phase conversion and further modification is required to recover acceptable image quality that is traditionally tackled using iterative techniques.

Direct modifications of the phase of the point-oriented object distribution provide an alternative means of realizing a robust CGH via the phase-seeded method. A modified quadratic object phase function is proposed that exceeds the necessary contrast ($C > 0.6$). Within the confines of the pattern geometries considered, this phase function may be precomputed in advance. The method has been shown to be applicable for a wide range of linear line patterns that traverse the annular rings of the seeded-phase function, though nonlinear shapes, such as annular rings, benefit to a lesser extent. The resulting reconstructions exhibit very high contrast, including the case of CGHs restricted to binary phase, and therefore offer practical exposure latitude for photolithography via a SLM or diffractive optical element. Comparisons to the IFTM-generated results indicated that comparable contrast performance is attainable for the case of a continuous phase CGH, while lower contrast was seen for the case of a binary phase CGH.

Efforts are now directed toward applying the point method to nonplanar patterns, where the object point ensemble is no longer confined to a single plane, and where the computational burden remains comparable to the planar case.

Funding. Engineering and Physical Sciences Research Council (EPSRC) (EP/G051887/1, EP/G051925/1).

REFERENCES

1. E. Buckley, "Holographic laser projection," J. Disp. Technol. **7**, 135–140 (2011).
2. C. Bay, N. Hubner, J. Freeman, and T. Wilkinson, "Maskless photolithography via holographic optical projection," Opt. Lett. **35**, 2230–2232 (2010).
3. R. W. Gerchberg and W. O. Saxton, "Phase determination for image and diffraction plane pictures in the electron microscope," Optik **34**, 275–284 (1971).
4. F. Wyrowski, E.-B. Kley, S. Buehling, T. J. Nellissen, L. Wang, and M. Dirkzwager, "Proximity printing by wave-optically designed masks," Proc. SPIE **4436**, 130–139 (2001).
5. J. J. Cowling, G. L. Williams, A. Purvis, R. McWilliam, J. J. Toriz-Garcia, N. L. Seed, F. B. Soulard, and P. A. Ivey, "Three-dimensional holographic lithography by an iterative algorithm," Opt. Lett. **36**, 2495–2497 (2011).
6. J. R. Fienup, "Phase retrieval algorithms: a comparison," Appl. Opt. **21**, 2758–2769 (1982).
7. J. J. Cowling, "An iterative algorithm for lithography on three-dimensional surfaces," Ph.D. thesis (Durham University, 2015).
8. C. Frere, D. Leseberg, and O. Bryngdahl, "Computer-generated holograms of three-dimensional objects composed of line segments," J. Opt. Soc. Am. A **3**, 726–730 (1986).
9. A. Maiden, R. McWilliam, A. Purvis, S. Johnson, G. L. Williams, N. L. Seed, and P. A. Ivey, "Nonplanar photolithography with computer-generated holograms," Opt. Lett. **30**, 1300–1302 (2005).
10. G. L. Williams, R. McWilliam, A. Maiden, A. Purvis, P. A. Ivey, and N. L. Seed, "Photolithography on grossly non-planar substrates," in *Conference on High Density Microsystem Design and Packaging and Component Failure Analysis* (IEEE, 2005), pp. 442–446.
11. R. McWilliam, A. Purvis, G. Williams, F. Soulard, and N. L. Seed, "High contrast patterns generated by phase-seeded CGH extensible to 3-D patterns and binary modulation," in *Digital Holography & 3-D Imaging Meeting*, OSA Technical Digest (Optical Society of America, 2015), paper DTh4A.4.
12. J. Rosen, "Computer-generated holograms of images reconstructed on curved surfaces," Appl. Opt. **38**, 6136–6140 (1999).
13. J. P. Waters, "Three-dimensional Fourier-transform method for synthesizing binary holograms," J. Opt. Soc. Am. **58**, 1284–1287 (1968).
14. P. Tsang, T.-C. Poon, W.-K. Cheung, and J.-P. Liu, "Computer generation of binary Fresnel holography," Appl. Opt. **50**, B88–B95 (2011).
15. Y. Takaki and M. Yokouchi, "Speckle-free and grayscale hologram reconstruction using time-multiplexing technique," Opt. Express **19**, 7567–7579 (2011).
16. F. Shen and A. Wang, "Fast-Fourier-transform based numerical integration method for the Rayleigh-Sommerfeld diffraction formula," Appl. Opt. **45**, 1102–1110 (2006).
17. A. K.-K. Wong, *Resolution Enhancement Techniques in Optical Lithography* (SPIE, 2001).
18. J. J. Toriz-Garcia, J. J. Cowling, G. L. Williams, Q. Bai, N. L. Seed, A. Tennant, R. McWilliam, A. Purvis, F. B. Soulard, and P. A. Ivey, "Fabrication of a 3D electrically small antenna using holographic photolithography," J. Micromech. Microeng. **23**, 055010 (2013).